High-current carbon-epoxy capillary cathode

J. Z. Gleizer,[1] T. Queller,[1] Yu. Bliokh,[1] S. Yatom,[1] V. Vekselman,[1] Ya. E. Krasik,[1] and V. Bernshtam[2]
[1]*Physics Department, Technion, Haifa 32000, Israel*
[2]*Department of Physics, Weizmann Institute of Sciences, 61000 Rehovot, Israel*

(Received 18 May 2012; accepted 14 June 2012; published online 24 July 2012)

The results of experiments on the reproducible generation of an electron beam having a high current density of up to 300 A/cm^2 and a satisfactorily uniform cross-sectional distribution of current density in a ~200 kV, ~450 ns vacuum diode with a carbon-epoxy capillary cathode are presented. It was found that the source of the electrons is the plasma formed as a result of flashover inside the capillaries. It is shown that the plasma formation occurs at an electric field $\leq$15 kV/cm and that the cathode sustains thousands of pulses without degradation in its emission properties. Time- and space-resolved visible light observation and spectroscopy analyses were used to determine the cathode plasma's density, temperature, and expansion velocity. It was found that the density of the cathode plasma decreases rapidly in relation to the distance from the cathode. In addition, it was found that the main reason for the short-circuiting of the accelerating gap is the formation and expansion of the anode plasma. Finally, it was shown that when an external guiding magnetic field is present, the injection of the electron beam into the drift space with a current amplitude exceeding its critical value changes the radial distribution of the current density of the electron beam because the inner electrons are reflected from the virtual cathode. © *2012 American Institute of Physics*. [http://dx.doi.org/10.1063/1.4739258]

I. INTRODUCTION

There is a continuous interest in cathodes that can be used for the generation of pulsed electron beams that have electron energy of $\varepsilon_e \geq 100$ keV, are uniform in the cross-sectional area at a current density $j_e \geq 100$ A/cm^2, and whose duration is $\tau_p \geq 10^{-7}$ s. These electron beams can be used to generate intense x-ray fluxes, to pump high-pressure gaseous lasers, and to generate powerful microwaves. A large required electron current density dictates that an electron diode be operated in the space-charge limited mode[1] with a relatively small anode-cathode (AK) gap of several mm. For instance, in order to obtain $j_e \sim 300$ A/cm^2 at an accelerating voltage of φ_{ac} ~300 kV, the value of the AK gap should be $d_{AK} \approx 1$cm in the case of a space-charge limited flow. Thus, the average electric field in the AK gap should be $E_{av} \sim 300$ kV/cm, which could lead to unpredictable electron emission from the cathode holder, if special measures are not taken to ensure its insulation. Here, let us note that to generate such high-current density electron beams a large cross-sectional area ($S > 10^3$ cm^2) electron diode, with a relatively small current density $j_e < 1$ A/cm^2 at its output can be used.[2] Such diodes are immersed in a guiding external magnetic field, which is used to focus the electron beam, producing high-current electron densities on a target placed at the desired location. The advantages of this method are: (a) a relatively small value of j_e in the diode, which allows one to operate with a larger d_{AK} value and, correspondingly, to decrease the value of E_{av}; (b) the possibility to generate an electron beam whose duration is rather long ($\tau_p \sim 10^{-4}$ s). However, this method requires a guiding magnetic field system and a rather long drift region in which the focusing of the electron beam occurs. Thus, in the majority of applications, high-current diodes are considered, whose operation is governed by the properties of the cathode electron source.

Field emission electron sources[3] provide extremely bright electron beams and these sources can be turned on and off practically simultaneously with the application of the accelerating voltage. However, in order to obtain $j_e \geq 100$ A/cm^2, one has to apply an electric field $E > 10^7$ V/cm and to maintain clean and high vacuum conditions. In addition, experimental data showed that the application of a pulsed electric field with $E > 10^7$ V/cm leads to an almost simultaneous formation of explosive emission (EE) plasma,[4] which terminates electron field emission and is accompanied by degasing processes and deterioration in the vacuum.

Thermionic electron sources[5] also cannot be considered as appropriate candidates for generating electron beams with a high-current density in pulsed diodes in spite of the fact that at present one can purchase thermionic cathodes with $j_e \geq 100$ A/cm^2.[6] The operation of these sources also requires high and pure vacuum conditions. In addition, even modern thermionic cathodes require heating to ~1500 K in order to achieve $j_e > 100$ A/cm^2, which leads to the necessity of applying powerful (several kW) external power supplies and special high-voltage de-coupling systems and time for heating and cooling of this type of electron source.

Thus, only electron sources based on rather dense plasma can be considered for generating pulsed electron beams with $j_e > 100$ A/cm^2 at a moderate accelerating voltage. Indeed, in order to obtain $j_e \sim 300$ A/cm^2 from the quasi-stationary boundary of the plasma, i.e., when the plasma electron saturation current density is equal to the current density dictated by the space-charge law, the density of the plasma should be $n_e \sim j_e/[e(k_B T_e/m_e)^{1/2}] \sim 6 \times 10^{13}$ cm^3 assuming plasma electron temperature, T_e, of a few eV,

where e and m_e are electron charge and mass, respectively, and k_B is the Boltzmann constant. The importance of stabilizing the emission plasma boundary is the key issue in pulsed high-current diodes. Generally, cathode plasma propagation with a typical ion sound velocity V_{pl} (for proton plasma with ion mass m_i and $T_e = 4\,\text{eV}$, $V_{pl} \approx (kT_e/m_i)^{1/2} \approx 2 \times 10^6\,\text{cm/s}$) toward the anode, results in a decrease in the effective AK gap, where the main potential difference occurs. Using a low impedance, high-voltage (HV) generator, leads to an increase in the average electric field and, correspondingly, in the extracted electron current density. In addition, transverse cathode plasma expansion increases the cross-sectional area, $S_{pl}(t)$, of the emitting plasma boundary and, correspondingly, increases the total emitted electron current. Finally, when the interaction of high-energy electrons with the anode results in a density energy deposition $\omega_e \geq 0.1\,\text{kJ/g}$, one obtains anode plasma formation[4,7] and, a corresponding ion emission toward the cathode. This ion emission switches the diode operation to bi-polar[1] mode, with a 1.86-fold increase in the electron current density due to partial compensation of the electron space charge in the cathode's vicinity, by the space charge of the ion flow. In addition, this anode plasma thermal expansion also leads to a decrease in the effective AK gap. One can estimate roughly the time of the anode plasma formation as $\tau_{pl} \approx \omega_e \rho_a \lambda_e / j_e \varepsilon_e \approx 100\,\text{ns}$, where $\rho_a \approx 9\,\text{g/cm}^{-3}$ is the specific density of an anode made of copper or stainless steel, $\lambda_e \approx 2\times10^{-3}\,\text{cm}$ is the typical electron mean free path, $j_e \approx 100\,\text{A/cm}^2$, and $\varepsilon_e \approx 200\,\text{keV}$. Thus, one can describe the time evolution of the electron current in a diode at time $t > \tau_{pl}$ as:

$$I_d(t) = 1.86 \times k \times S_{pl}(t)\frac{4}{9}\varepsilon_0\left(\frac{2e}{m_e}\right)^{1/2}\frac{[\varphi_g(t) - I_d(t)Z_g]^{3/2}}{(d_{AK} - 2V_{pl}t)^2} \times \left[1 + \left(\frac{m_e}{m_i}\right)^{1/2}\right],$$

where $k > 1$ is the coefficient that considers the increase in the space-charge limited electron/ion current density due to deviation from the diode planar geometry, i.e., so-called edge effects,[8–10] and φ_g and Z_g are the HV generator output voltage and impedance, respectively.

There are two main categories of plasma source: active and passive.[11,12] In an active plasma source, the cathode plasma is formed prior to the application of the accelerating pulse, whereas in passive plasma sources it is formed by an accelerating pulse applied to the diode. The advantage of an active plasma source is that one can control the parameters of the plasma (density, temperature, and expansion velocity). However, when these sources are applied, additional power supplies and HV decoupling elements are needed. In general, this type of electron source consists of a plasma source located inside a cathode cavity that has an output grid to stabilize the plasma emission boundary. Several plasma sources were investigated during the last decades for the generation of electron beams with $j_e < 100\,\text{A/cm}^2$ (see, for instance review of active plasma sources, Ref. 13). Here we briefly review only the ferroelectric plasma source[14,15] (FPS) and hollow anode[16,17] (HA) plasma sources, which have features similar to those of other active plasma sources from the point view of electron beam extraction.

In FPS, the plasma generation occurs due to ionization of desorbed and sputtered gas and bulk material by electron avalanching along the ferroelectric surface, in the tangential component of the electric field of a driving pulse, whose amplitude is a few kV, that is applied between the strip-like front and rear solid electrodes, (the average normal component of the electric field is in the range is 10 – 25 kV/cm). It was shown that the parameters of the plasma in the vicinity of the ferroelectric surface can be controlled in a rather broad range, i.e., $n_e = 10^{11} - 10^{15}\,\text{cm}^{-3}$, $T_e = 1 - 8\,\text{eV}$, by the amplitude and form of the driving pulse and the properties of the ferroelectric.[14,15] The process of surface plasma generation is accompanied by this plasma expansion toward the cathode output grid and pre-filling of the AK gap by the dilute plasma prior to the application of the accelerating pulse. Thus, at the beginning of the accelerating pulse one obtains "cleaning" of the AK gap of this dilute plasma, so-called plasma pre-filled mode of the diode operation.[1,17] Later in the accelerating pulse, electron beam generation, with a current density determined by the space-charge law, occurs from the plasma boundary fixed in the vicinity of the cathode output grid. These plasma sources were used successfully to generate electron beams with $j_e \leq 50\,\text{A/cm}^2$, $\tau_p \leq 300\,\text{ns}$ and a cross-sectional area up to 100 cm^2.[18,19]

The HA with an incorporated FPS was also successfully used to generate electron beams with $j_e < 50\,\text{A/cm}^2$.[20] The operation of the HA has the following sequences. First, a driving pulse is applied to the FPS placed at the bottom of the cylindrical HA, which causes surface plasma to be generated and to expand. When this relatively dilute plasma reaches the HA wall, a main discharge is initiated by an additional pulsed generator between the FPS front electrode and the HA walls. This discharge forms a relatively dense plasma ($\sim10^{12}\,\text{cm}^{-3}$) which fills the entire HA volume and penetrates through the HA output high transparency grid, into the AK gap. At the time when the density of the HA plasma in the vicinity of the output grid reaches the desired value, an accelerating pulse, produced by a HV pulsed generator, is applied to the HA (at that time the HA becomes the cathode of the diode). This leads first to the plasma prefilled mode of the diode operation, followed by electron extraction from the plasma boundary located at the HA output grid. In order to decrease the plasma pre-filling of the AK gap, an auto-bias of the HA output grid was used.[21] This HA was used in order to generate a large cross-sectional area ($\sim$100 cm^2) electron beam with $j_e \leq 35\,\text{A/cm}^2$.[16]

Both of these active plasma sources, as well as other similar plasma sources,[13] operate in moderate vacuum conditions (1–10 mPa), allowing electron beams to be generated with a total current amplitude up to several kA, satisfactory uniform cross-sectional current density distribution, and pulse duration of several hundreds of ns at accelerating voltages of several hundreds of kV. However, the application of these active plasma cathodes to generate electron beams with $j_e > 100\,\text{A/cm}^2$ is severely restricted. Indeed, in the

active plasma source, when fast extraction of electrons from the plasma occurs, the latter acquires a positive potential because of the plasma ions' slow response. For instance, it was shown that when the current amplitude of the extracted electron beam reaches $\sim$1 kA ($j_e \leq 30$ A/cm^2), the plasma potential rises up to $\sim$6 kV.[17,22] When the extracted current has a larger amplitude, the increase in the plasma positive potential could reach even tens of kV. This leads to an increase in the energy of the plasma ions accelerating in the sheath that is formed between the plasma and output grid and cathode walls. These energetic ions form plasma spots at the grid surface and on the inner surface of the cathode structure. These plasma spots become the source of electrons that lead to the non-uniformity of the extracted electron beam. Thus, active plasma sources also cannot be considered appropriate candidates for generating electron beams with $j_e > 100$ A/cm^2 and a total current amplitude of a few kA.

Now let us consider briefly passive plasma sources, namely EE and flashover plasmas, which can serve as almost unlimited electron sources due to the high density ($n_e > 10^{14}$ cm^{-3}) of the plasma. EE plasma appears as a result of the fast phase transitions of micro-protrusions that always exist at the cathode surface.[4] At the apexes of these micro-protrusions, one obtains an enhancement of the applied electric field, which causes an exponential increase in the field emission current density, and a corresponding fast increase in the temperature of the micro-protrusion and the transformation of the field emission to thermionic emission. The latter allows electron emission to increase, which leads to a further increase in the temperature of the apex, its melting, and evaporation, and to dense plasma formation due to ionization of vapors by emitted electrons. Depending on the amplitude of the electric field and on the properties of the cathode material, one can estimate the time delay in the plasma formation as[23] $\tau_d \approx \rho\chi\sigma_0 \ln(T_{cr}/T)\int_0^t j_e^2(t)dt$, where T_0 and T_{cr} are the initial temperature and critical temperature at which the explosion of the material occurs, respectively, σ_0 is the initial conductivity of the material, and χ is the specific energy necessary for the material to melt. Estimates show that in order to obtain a $<$10 ns time delay in the formation of the explosive plasma, the value of j_e flowing through the micro-protrusion should be in the range $(2–6) \times 10^8$ A/cm^2. In addition, EE is accompanied by cathode erosion at a typical rate of $\sim 10^{-4}$ g/C, which leads to vacuum deterioration when the diode is operated at a high repetition rate. The main obstacle in the application of EE plasma is its fast ($>10^6$ cm/s) expansion velocity because of large density gradients. Indeed, the plasma density decreases drastically away from the vicinity of the explosive center, from $\sim 10^{19}$ cm^{-3} at a distance of $\sim$30 μm to $\sim 10^{18}$ cm^{-3} at a distance of $\sim$100 μm.[23] Other obstacles to the use of EE plasma are its cross-sectional non-uniformity and the time delay in this type of plasma generation in the case of a moderate accelerating voltage amplitude ($\leq 10^5$ V/cm) and rise time [$dE/dt \leq 5 \times 10^{12}$ V/(cm·s)].[24] In fact, the phenomenon of EE was revealed and explained by Mesyats and co-authors[4,25,26] but they do not consider the time dependence of the appearance of EE sources in relation to the rise time of the accelerating pulse. However, experimental results[24,27] showed that the uniformity and time delay in the explosive plasma emission depend not only on the value of the applied electric field but also strongly on the rise time of the accelerating voltage. Thus, one should consider that in the case of a fast rising [$dE/dt > 10^{13}$ V/(cm·s)] electric field, the mechanism of the cathode plasma formation involves not the explosion of micro-protrusions but flashover plasma. Indeed, the existence of dielectric micro-inclusions at the surface of the cathode can lead to dielectric surface flashover and, correspondingly to plasma formation.[23] In order to achieve effective flashover, one has to apply an electric field with a large dE/dt in order to achieve effective polarization of the dielectric inclusion which causes flashover. In addition, dielectric flashover can be realized by the plasma ion flow, which causes charging of the dielectric followed by an electrical surface breakdown. Thus, one can conclude that the application of an EE cathode at a moderate value and rise time of the accelerating voltage is problematic for the generation of electron beams with uniform cross-sectional current density distribution and pulse duration $>10^{-7}$ s.

The flashover plasma formed at the surface of the cathode was extensively investigated in cathodes made of different types of velvet and carbon fibers, and in metal-ceramic and multi-capillary cathodes.[28–43] In general, these types of cathodes are characterized by surface flashover plasma formation in the nanosecond timescale due to the fast polarization of the dielectric or metal high-resistive fibers.[27] That is, the flashover process occurs due to the charging of the individual fiber's "stray" capacitance by the displacement current, dE/dt. When the value of dE/dt is larger than the sum of the emitted current and the leakage surface current, the induced potential difference initiates a surface discharge and, correspondingly, plasma formation. Experiments with different types of such cathodes (velvet and carbon fiber, multi-capillary, and metal-ceramic cathodes) using different types of time- and space-resolved optical, spectroscopic, electrical, and x-ray diagnostics, showed that the formation and uniformity of this type of plasma depend strongly on the value and rise time of the accelerating voltage.[24,42] Namely, the larger the value of dE/dt, the faster is the formation and uniformity of the plasma. In fact, the plasma formation on the surface of carbon and velvet fiber cathodes is characterized by many bright spots, which are satisfactorily uniformly distributed at the beginning of the accelerating pulse and redistributed during the accelerating pulse to the periphery of the cathode due to the edge effect. The latter allows a larger current density at locations having a larger electric field. Nevertheless, these cathodes have demonstrated their excellent operation characteristics: fast turn-on, i.e., plasma formation starts at $E \sim 10$ kV/cm; uniform cross-sectional electron beam distribution; long lifetime; low out-gassing; and relatively low velocity of the plasma expansion. These features of the carbon and velvet fiber cathodes operation allow one to obtain almost constant diode impedance. These cathodes were used to generate electron beams with a current density $<$50 A/cm^2 and cross-sectional area up to several m^2. However, efforts to use the same cathodes to generate

electron beams with a current density $>100\,A/cm^2$ and pulse duration $>100\,ns$ failed, because of the damage incurred by these cathodes ($<10^3$ of generator shots) and fast AK gap plasma shorting. The short lifetime of these cathodes is related to the formation of several hot plasma spots that supply the main part of the electron emission; the plasma of these spots expands fast, leading to the AK shorting. This concern applies also to other types of active plasma sources. That is, the formation of hot spots on the surface of the cathode or cathode output grid leads to denser plasma formation, which supplies a larger current density and, correspondingly, obtains a higher temperature due to Joule heating. This leads to a decrease in the plasma resistivity and a larger current which starts to flow in this region. This self-consistent process leads to faster plasma propagation in that location and shorting of the AK gap. Thus, the application of this type of cathodes for the generation of high-current electron beam with current density $>100\,A/cm^2$ and pulse duration $>100\,ns$ is also problematic.

To summarize this introduction, one can conclude that at the present there is no reliable and long life-time electron source which can be used for the generation of an electron beam with $j_e \geq 100\,A/cm^2$ at an accelerating voltage of several hundreds of kV and $\tau_p > 100\,ns$. In this paper, we describe the results of experiments with a carbon-epoxy capillary cathode, which was used to generate electron beams with a current amplitude up to 2.5 kA, $j_e \approx 300\,A/cm^2$ and $\tau_p \approx 400\,ns$, at an accelerating voltage of $\varphi_{AK} \leq 200\,kV$. Using different time- and space-resolved electrical, optical, x-ray and spectroscopic diagnostics, it was found that this type of cathode outperforms those made of carbon fiber or velvet.

II. EXPERIMENTAL SETUP

The experimental setup is shown in Fig. 1. The cathode is made of 76 carbon-epoxy capillaries ("Van Dijk Pultrusion Products") having almost infinite resistivity. These capillaries were uniformly distributed and fixed in an aluminum holder, 3 cm in diameter. The external and internal diameters of each capillary are 1.5 mm and 0.7 mm, respectively, and the distance between the centers of neighboring fibers is 3 mm. In the experiments, two cathode designs were tested. In the first, a screening electrode was not used and, in order to decrease the edge effect, the length of the capillaries was reduced toward the cathode's periphery, i.e., the cathode had a sphere-like form (see Fig. 1(a)). In the second design, equal lengths of carbon-epoxy capillaries were used with a screening electrode (see Fig. 1(b)) made of aluminum coated with 100 μm-thick Al_2O_3 ceramics.

Electron beam generation was studied in a vacuum diode immersed in an axial external guiding magnetic field, whose purpose was to prevent a large electron divergence and possible electron emission from the cylindrical surface of the cathode holder. The anode was made of a stainless steel grid having 50% transparency and cell size of 970 μm × 970 μm. In the experiments, the value of the AK gap d_{AK} was varied in the range 8–15 mm.

The cathode and anode were placed inside a vacuum stainless steel tube, 90 mm in diameter and 700 mm in length, and having windows for optical access. Two turbomolecular pumps were used to produce a 2×10^{-5} Torr vacuum in the tube. An external axial guiding magnetic field of ~3 kG with a half period duration of 400 μs was produced by a solenoid, consisting of five coils connected in series and supplied by a 600 μF, 2 kV capacitor bank. This magnetic field was sufficient to magnetize the electron beam (electron Larmor radius $r_L \leq m_e c(\gamma^2 - 1)(eB)^{-1} \approx 5.5\,mm$, where $\gamma = 1.4$ is the relativistic factor for an accelerating voltage of 200 kV, $B = 0.3\,T$ and c is the light velocity). The axial uniformity of the magnetic field was checked using a calibrated Hall probe and was found to be in the range of ±10% along a 30 cm distance with respect to the anode grid.

The diode was powered by a 12-stage pulsed forming network HV generator (≤200 kV, ~50 Ω, ≤450 ns),[41] which was triggered by a Maxwell generator (model 40230) when the external magnetic field reached its maximal value. The diode voltage φ_{AK} and current I_d were measured using an active voltage divider and self-integrated Rogowski coil, respectively, and the electron beam current I_b was measured by a movable low-inductance Faraday Cup (FC) placed inside the drift tube at different distances behind the output anode grid. The FC had an entrance hole 54 mm in diameter, covered by a high transparency (~80%) stainless steel grid.

The light emission of the plasma formed at the carbon-epoxy capillaries surface (side and front views) was studied using a fast framing 4Quik05A camera. For the front view, in order to avoid beam electron interaction with the perspex window placed at the output of the drift tube, two permanent magnets were installed at that location (see Fig. 1(a)). The

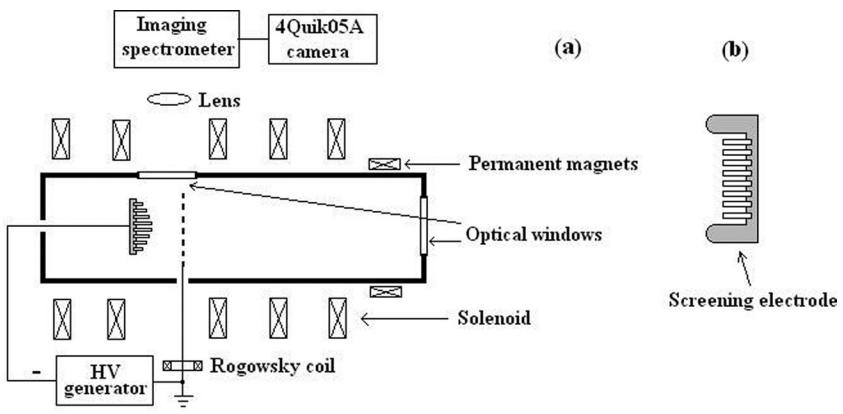

FIG. 1. (a) Experimental setup. (b) Carbon fiber-epoxy cathode with a screening electrode.

uniformity of the radial distribution of the electron beam current density was checked by an array of eight collimated Faraday cups (CFCs). The diameter of the entrance hole of each CFC was 1 mm. In addition to the CFCs' measurements, the cross-sectional distribution of the electron beam current density at different distances from the grid anode was checked by x-ray imaging of the movable collector. In this case, a 100 μm-thick Mo foil collector, to which was attached a 2 mm-thick EJ200 fast plastic scintillator, was used. Electron beam interaction with Mo foil causes x-ray generation, which produces a luminescence pattern of the electron beam in the attached scintillator, and this pattern is captured by the fast framing camera.

The cathode and anode plasma parameters (density, temperature, and expansion velocity) were studied using visible time- and space-resolved spectroscopy. The measurements were made using a 750 mm Jobin Yvon spectrometer (2400 grooves/mm grating, spectral resolution of ~0.1 Å/pix). The light emission from the plasma was collected through a Plexiglas window by a lens which focused the input spectrometer slit to the desired location inside the AK gap (see Fig. 1(a)). The spectral line images at the output of the spectrometer were recorded by a 4Quik05A framing camera. In the experiments, when the time evolution of the different spectral lines was studied at different distances from the cathode, a photomultiplier tube (PMT Hamamatsu R1617) was used. The PMT was placed behind a slit (observable spectral range of ~10 Å) which was mounted at the spectrometer output. The calibration of the optical system was carried out using Oriel spectral lamps.

III. EXPERIMENTAL RESULTS

A. General parameters of the diode

Typical waveforms of the diode voltage, current, and electron beam current, measured by the FC at a distance of ~5 cm from the anode grid are shown in Fig. 2. In general, the diode current temporal behavior is governed by the space-charge law. However, when one wants to simulate this current behavior, several additional and not well defined processes should be considered. Namely, one has to include the time-dependent cross-sectional area of the emitting plasma boundary due to its

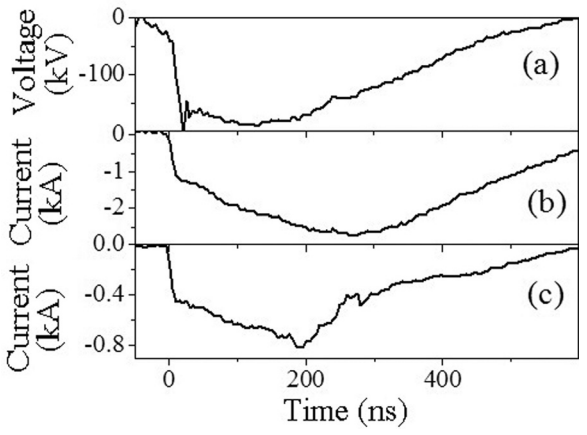

FIG. 2. Typical waveforms of the diode voltage (a), diode current (b), and electron beam current (c). $B \approx 3$ kG, $d_{AK} \approx 1.5$ cm, the distance from the anode grid to the Faraday cup is of 5 cm.

expansion across the magnetic field, and the decrease in the effective AK gap because of the cathode plasma expansion toward the anode.[4,41] Here, let us note that both the radial and axial plasma expansion velocities could be time-dependent because of the change in the plasma gradients during plasma expansion. In addition, one has to take into account the electric field enhancement at the emitting boundary of the plasma, which also changes during the accelerating voltage. Finally, one has to include in this calculation effects related to the anode plasma formation, which is determined by the electron beam energy density deposition into the anode grid. In the present experiments, the appearance of this anode plasma is delayed by $\tau_d \sim 100$ ns with respect to the beginning of the accelerating voltage when the electron energy density deposition becomes ≥ 0.1 kJ/g. The anode plasma expansion toward the cathode also leads to a decrease in the AK gap. In addition, ion emission from the anode plasma boundary partially compensates the space-charge of emitted electrons. Thus, it is difficult to make a simulation of the diode current without precise knowledge of the time evolution of the above described processes of the cathode and anode plasma evolution. Nevertheless, one can estimate roughly that the average expansion axial velocity of both the anode and cathode plasmas does not exceed $\bar{V}_{pl} \approx 2.7 \times 10^6$ cm/s taking into account that the duration of the HV phase of the diode operation does not exceed 550 ns. In the experiments with $d_{AK} = 1$ cm, the HV pulse duration was found to be $\tau_p \approx 450$ ns, which results in an even lower value of $\bar{V}_{pl} \leq 2.2 \times 10^6$ cm/s. Here, let us note that the waveform of the electron beam current follows the waveform of the diode current until $\tau_d \sim 200$ ns. Later in the accelerating pulse, one obtains a significant decrease in the amplitude of the electron beam current. This can be explained by neutralization of the electron beam space charge by co-moving ions emitted from the anode plasma that is formed at that time.

As one can see in Fig. 2, the electron emission starts almost simultaneously with the beginning of the accelerating voltage, i.e., at $\varphi_{AK} \approx 30$ kV, which corresponds to an average value of $E_{av} \approx 20$ kV/cm. Such a low electric field threshold, sufficient for the beginning of the electron emission, is typical for the flashover plasma which can be formed on the surface of the carbon fiber-epoxy as a result of a large value of $dE/dt \approx 10^{13}$ V/(cm·s).[24] The amplitude of the diode current reaches $I_d \approx 2.8$ kA which corresponds to a rather large average value of $\bar{j}_e \approx 385$ A/cm^2 for the plasma emitting area of ~7 cm^2.

One of the important properties of the electron diode is its impedance behavior. In Fig. 3, the temporal dependence of the diode impedance $Z_d = \varphi_{AK}/I_d$ at $B \approx 3$ kG and $d_{AK} \approx 11$ mm is shown. For comparison, the impedance of the diode with a velvet cathode measured in the same experimental conditions is shown as well. One can see that when carbon fiber-epoxy and velvet cathodes are used the value of Z_d decreases from $Z_d \approx 90$ Ω and $Z_d \approx 75$ Ω at the beginning of the accelerating pulse down to $Z_d \approx 18$ Ω and $Z_d \approx 45$ Ω at $\tau_d \approx 450$ ns, respectively. The smaller value of Z_d at $\tau_d \approx 50$ ns for the velvet cathode can be explained qualitatively by faster flashover plasma formation at its surface and a larger amount of plasma spots as compared with the carbon fiber-epoxy cathode.[24] The significant, ~2.5 times smaller value of Z_d at $\tau_d \approx 450$ ns for the carbon fiber-epoxy cathode can be

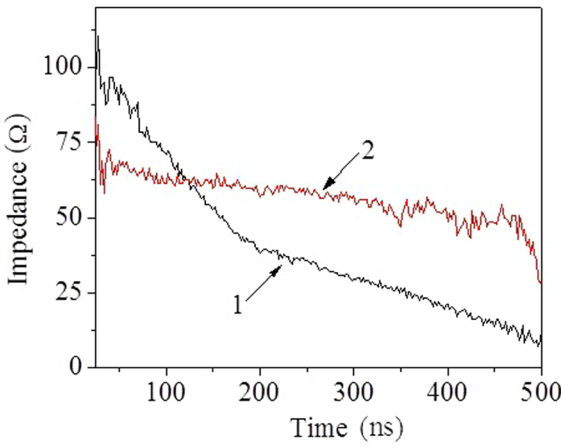

FIG. 3. Diode impedances: 1 – carbon-epoxy capillary cathode; 2 – velvet cathode. $B \approx 3$ kG, $d_{AK} \approx 11$ mm, $\phi_{AK} \approx 160$ kV.

explained by a faster cathode plasma expansion toward the anode than in the case of the velvet cathode. In the latter case, an average total (cathode and anode) plasma expansion velocity can be estimated as $\bar{V}_{pl} \leq 2 \times 10^6$ cm/s. Here let us note that the impedance of the diode with velvet cathode was obtained in the first few shots of the generator, because as it will be shown below, the emission properties of the velvet cathode deteriorate rather fast along the number of shots. In addition, during the 450 ns of the accelerating pulse, the energy delivered to the diode by the HV generator was ~70% of the stored energy. The remaining ~30% of the stored energy was dissipated in the discharge gaps and in the Joule heating of the plasma when the diode shot-circuit occurred.

Let us note that the rate of the decrease in diode impedance is $dZ_d/dt \approx 3.4 \times 10^8$ Ω/s during the first 250 ± 30 ns of the accelerating pulse, and it becomes significantly slower, $dZ_d/dt \approx 10^8$ Ω/s, in the remaining part of the accelerating pulse. This temporal behavior of the diode impedance can be explained by the cathode plasma transverse and axial expansion. The plasma flows generated by the expansion of separate capillaries in the transverse direction leads to overlapping of these flows and, to a corresponding increase in the emission plasma boundary and the amplitude of the emitted electron current. In addition, as will be shown later, the plasma expansion toward the anode leads to a drastic decrease in the plasma density. Thus, one can suppose that the fast decrease in the diode impedance obtained at the beginning of the accelerating pulse is related primarily to the increase in the plasma emitting area.

The study of the lifetime of the carbon fiber-epoxy cathode showed that after ~4000 generator pulses at an average current density of $\bar{j}_e \approx 340$ A/cm^2 (in these experiments the AK gap was $d_{AK} = 11$ mm), the amplitude of the diode current and voltage did not change, and the carbon-epoxy fibers incurred no visible damage (see Figs. 4(a) and 4(b)). In the same experimental conditions, the test of the velvet-based cathode already showed a drastic decrease in the diode current within 200 generator pulses, and after 1000 pulses the amplitude of I_b decreased by 1.6 times, from 2.4 kA up to 1.5 kA (see Fig. 4(c)). Moreover, a visual inspection of the velvet revealed severe damage in the form of several burned spots, with a diameter of several mm at the surface of the

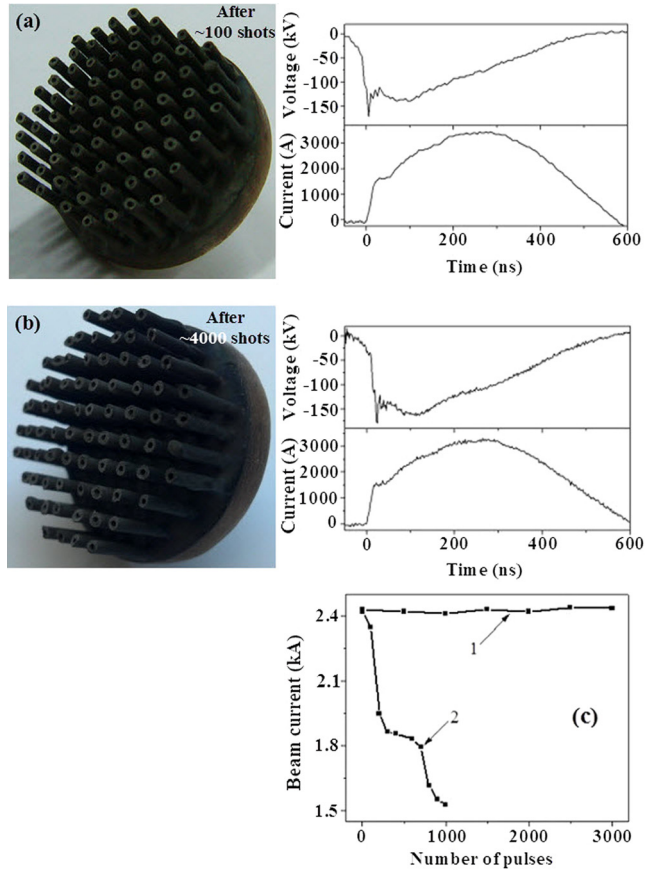

FIG. 4. Photos of the carbon-epoxy capillary cathode and typical waveforms of the diode voltage and current (a) after ~100 and (b) ~4000 generator shots. (c) Dependence of the electron beam current measured by the FC cup at the distance of 5 mm behind the anode grid on the number of accelerating pulses: 1 – carbon-epoxy capillary cathode; 2 – velvet cathode. $B \approx 3$kG, $d_{AK} \approx 1.1$ cm, $\varphi_{AK} \approx 145$ kV.

velvet. The reason for this damage could be the nonuniformity of the plasma, which led to an extremely large current density at these locations. Thus, velvet cannot be considered as a long-life electron source for the generation of an electron beam with $j_e > 100$ A/cm^2.

In addition to the velvet cathode, the carbon-epoxy capillary cathode was compared with carbon and aluminum cathodes in the same experimental conditions. These cathodes have a cylindrical form with rounded edges and concentric grooves at the emitting surface. Typical waveforms of the diode voltages obtained at $d_{AK} \approx 1$ cm with carbon fiber-epoxy capillaries and Al cathodes are shown in Fig. 5. One can see a spike in the voltage for the Al cathode (a similar spike was also observed for the carbon cathode) that demonstrates also an increase in the time delay in the beginning of the electron emission. Indeed, in the case of the Al cathode, the beginning of the electron emission was delayed by 15 ± 5 ns as compared with that of the carbon-epoxy capillary cathode. In addition, one can see a significant decrease in the duration of the voltage pulse in the case of the Al cathode (~500 ns) as compared with that of the carbon-epoxy capillary cathode (~580 ns). For the carbon cathode, the voltage pulse duration was also ~500 ns. The shorter duration of the accelerating pulse for the Al or carbon cathodes can be explained by the faster expansion velocity of the

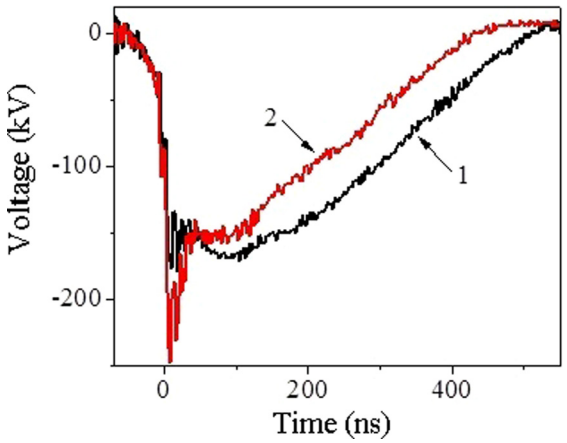

FIG. 5. Typical waveforms of the diode voltage: 1 – carbon-epoxy capillary cathode, 2 – Al cathode. $d_{AK} \approx 1$ cm.

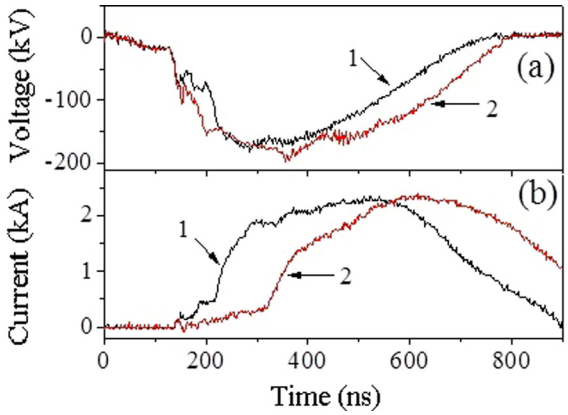

FIG. 6. Typical waveforms of the diode voltage (a) and current (b). 1 – carbon-epoxy capillary cathode; 2 – Al cathode. $d_{AK} \approx 1$ cm.

cathode and anode plasmas. In Sec. III B, it will be shown that these data relate to a smaller amount of plasma spots formed at the surface of the Al and carbon cathodes and, correspondingly, to a larger current density supplied by each plasma spot. The latter requires that the plasma at that location have higher temperature and density values, which results in faster plasma expansion velocity.

In order to test the dependence of the time delay in the electron emission on the accelerating voltage rise time, $d\varphi_{AK}/dt$, the value of $d\varphi_{AK}/dt$ was increased from 20 ns up to 280 ns by an increase in the gas pressure inside the HV generator spark gap tube. It was found that this increase in $d\varphi_{AK}/dt$ results in a ~100 ns time delay in electron emission in the case of the Al cathode as compared with the carbon-epoxy capillary cathode (see Fig. 6). These data indicate a different phenomenon that governs the electron emission in the case of carbon fiber-epoxy and Al or carbon cathodes. For the carbon fiber-epoxy flashover plasma can be generated even for a slow rise-time of the accelerating pulse due to the high resistance of the fiber. However, the formation of explosive emission plasma or flashover plasma on micro-protrusions or dielectric inclusions on the surface of Al or carbon cathodes requires significantly larger values of $d\varphi_{AK}/dt$.

Thus, the experimental results presented in this subsection showed that the carbon-epoxy capillary cathode outperformed the commonly used explosive emission cathodes (larger time delay in turn-on and faster plasma expansion velocity) and flashover plasma velvet cathode (shorter life-time).

B. Light and x-ray emission measurements

1. Front view light images of the cathode plasma

Typical front, light emission images, obtained with the carbon-epoxy capillary cathode (see Fig. 1(a)) at different time delays with respect to the beginning of the accelerating pulse are shown in Figs. 7(a)–7(d). One can see that almost all the fibers emit a bright light already at $\tau_d \approx 50$ ns with

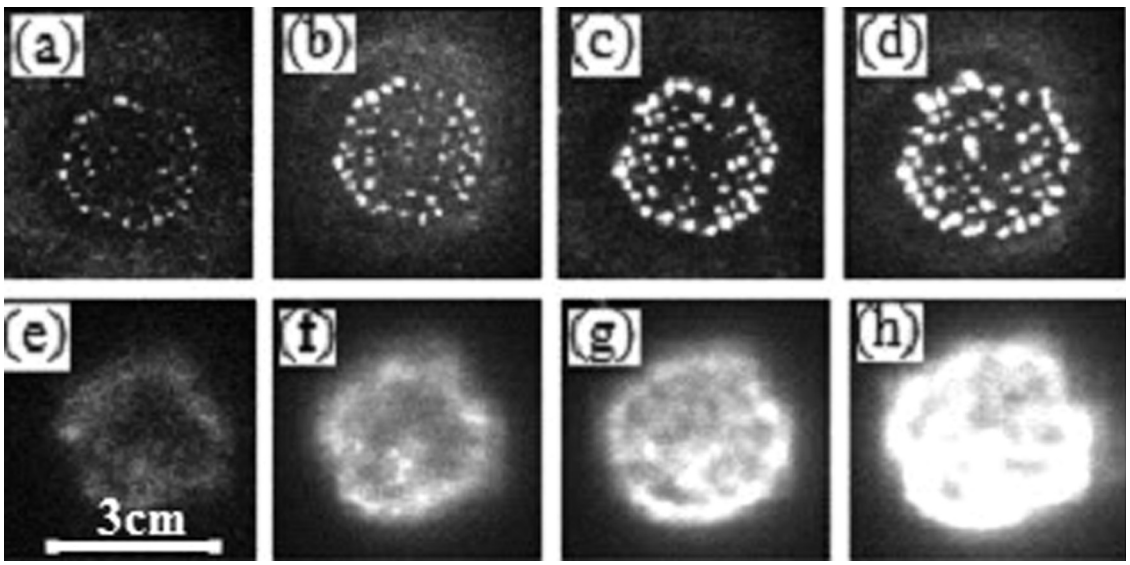

FIG. 7. (a)-(d) Typical front image of light emission from the carbon-epoxy capillary cathode, (e)-(h) typical x-ray image of the electron beam. (a) and (e) $\tau_d \approx 50$ ns; (b) and (f) $\tau_d \approx 80$ ns; (c) and (g) $\tau_d \approx 130$ ns; (d) and (h) $\tau_d \approx 180$ ns. The frame duration was 20 ns. A Mo foil collector was placed behind the anode grid, $B \approx 3$ kG, $d_{AK} = 1$ cm, $\varphi_{AK} \approx 150$ kV. The cathode is shown in Fig. 1(a).

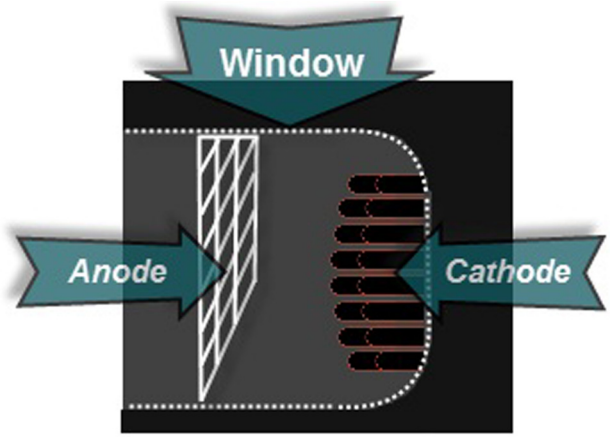

FIG. 8. Schematic drawing of the AK gap view point.

maximal intensity at the peripheral capillaries. The number of these emission centers does not change during the accelerating pulse and only the diameters of these bright spots are increased due to radial plasma expansion. Let us note that spots of much lower intensity were already obtained at $\tau_d \approx 30$ ns ($E_{av} \approx 15$ kV/cm), which agrees well with the beginning of electron emission and with the appearance of the light and electron emission in the case of the velvet cathode which was tested in the same experimental conditions. The increase in the magnification of the framing camera allows one to obtain a weak light emission from the location between the fibers at $\tau_d > 150$ ns. The latter can be related to the plasma expansion across the magnetic field, which should lead to an increase in the cross-section of the plasma emission area. The Bohm diffusion coefficient for the plasma expansion in the transverse direction, which can be estimated as $D_\perp = ck_BT_e/16eB = 6.25 \cdot 10^6 T_e B^{-1} \approx 10^4 \text{cm}^2/\text{s}$, results in the plasma expansion distance $\delta = \sqrt{D_\perp t} \approx 0.66$ mm during $t = 200$ ns. Thus, within ~200 ns of the accelerating pulse one can expect overlapping of the plasma flows that are formed at neighboring fibers.

2. Side view light images of the light emission

A drawing of the AK gap viewed from the side through the Perspex window is presented in Fig. 8. Side-view framing images of the light emission were obtained at different values of τ_d and at a small angle with respect to the normal to the AK axis in order to distinguish anode light reflections from actual anode plasma spots.

The motivation behind these measurements was to determine the location where the cathode plasma occurs, i.e., either on the internal or external cylindrical surface of the carbon-epoxy capillary. Fig. 9 presents these light images taken at different values of τ_d. One can see that during the entire 500 ns of the HV pulse there are no signs of dense plasma on the external surface of the capillaries, while on the edges of the capillaries obvious plasma spots are visible throughout the entire HV pulse. Since the cathode's capillaries are made of an insulating material, one can state that the plasma is generated by a surface flashover that occurs inside the capillary, similar to that shown in the case of the multi-capillary dielectric cathode.[49] In addition, the steep decay of the light emission of the cathode plasma spots in relation to the distance from the cathode indicates a fast decrease in the cathode plasma density. These data are in qualitative agreement with the spectroscopic measurements described in Secs. III C 1 and III C 2. The weak light emission from the anode grid at $\tau_d < 150$ ns is related to the light emitted by the cathode plasma and reflected by the anode. However, at $\tau_d \geq 150$ ns one obtains generation of anode plasma spots, the intensity of which increases during the accelerating pulse. At $\tau_d \geq 350$ ns the intensity of the anode spots becomes brighter than the cathode plasma luminosity. These data indicate formation of rather dense and hot anode plasma. During the voltage pulse, this plasma propagates towards the cathode and at $\tau_d \geq 450$ ns one obtains overlapping between anode and cathode plasmas that coincides with the termination of the accelerating pulse and the beginning of the ringing in the diode current, i.e., with the short-circuiting of the diode. Thus, one can conclude that the rea-

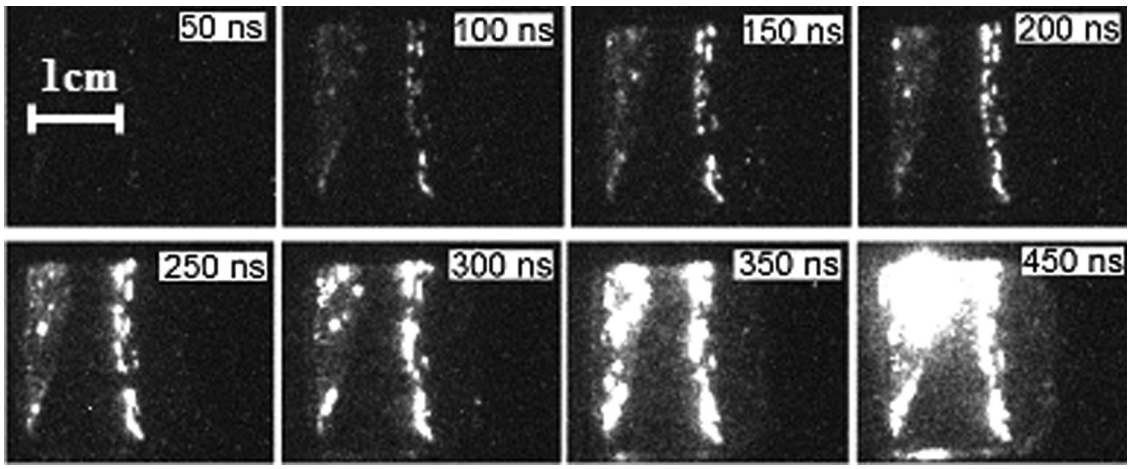

FIG. 9. Side view framing images of light emission from the cathode and anode plasmas at different time delays with respect to the beginning of the accelerating pulse. $B \approx 3$ kG, $d_{AK} = 1$ cm, $\varphi_{AK} \approx 150$ kV. The cathode is shown in Fig. 1(a).

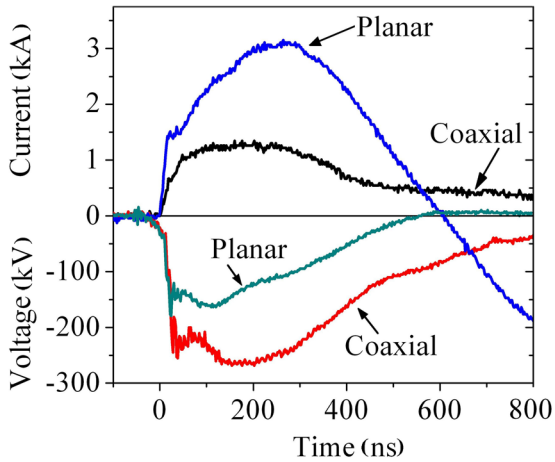

FIG. 10. Typical waveforms of the diode current and voltage in the cases of planar and magnetically insulated coaxial diodes with carbon-epoxy capillary cathode. $B \approx 3$ kG, $d_{AK} = 1$ cm.

son for the diode shortening is the formation and propagation of the anode plasma, while the expansion of the cathode plasma plays a minor role in this process.

In order to check this conclusion, the anode grid was removed, which resulted in a magnetically insulated coaxial diode setup. This diode generates a cylindrical hollow electron beam which propagates in the axial direction and has an azimuthal drift in the $\boldsymbol{E}_r \times \boldsymbol{B}_z$ fields. Typical waveforms of the diode current and voltage when planar and coaxial diodes were used are shown in Fig. 10. One can see that the amplitude and duration of the accelerating pulse increases significantly in the case of the coaxial diode, and calculations showed that almost all the energy stored in the HV generator was delivered to the diode and transferred to the energy of the electron beam. Framing images of the light emission from the cathode plasma in the case of the coaxial diode (see Fig. 11) showed that the cathode plasma light emission also remains close, <2 mm, to the edges of the capillaries. In addition, one can see that the plasma formation occurs mainly at the capillaries located at the cathode's periphery where the largest electric field is realized. The amplitude of the diode current reached $\sim$1.2 kA, which gives an average current density of 400 A/cm^2 for the plasma emitting area of $\sim$3 cm^2.

Cross-sectional uniformity of the electron beam was studied using x-ray imaging and an array of CFCs. Typical x-ray images of the electron beam generated in the diode when using the carbon-epoxy capillary cathode (Fig. 1(a)) demonstrate a satisfactorily uniform electron beam current density even at the beginning of the accelerating pulse when separate plasma flows do not yet overlap each other (see Figs. 7(e)–7(h)). This can be explained by divergence of emitted electrons, which results in a relatively large Larmor radius ($\leq$5 mm). For comparison, the cathode plasma light emission and x-ray images of the electron beam generated by the carbon and Al cathodes in the same experimental conditions are shown in Fig. 12. One can see significantly worse uniformity of the light emission and cross-sectional current density distribution than that obtained with the carbon fiber-epoxy cathode. The diameter of the electron beam guided by a magnetic field $B \approx 3$ kG (see Figs. 7(e)–7(h)), obtained by x-ray images, was $\sim$3.5 cm, i.e., approximately equal to the cathode's diameter. In the same experimental conditions, using the set of eight CFCs the electron current density radial distribution was fitted by Gaussian distribution with a full width at half maximum (FWHM) of $\sim$15 mm (see Fig. 13) and maximal value of $j_e \approx 175$ A/cm^2.

The test of the cathode design, shown in Fig. 1(b), with a flat carbon fiber-epoxy surface and screening electrode, showed similar features of light emission from the cathode surface, namely bright emission spots at the apexes of the carbon fiber-epoxy capillaries. However, in this case, bright emission spots at the cathode periphery were not observed, due the screening electrode (see Fig. 14(a)), the application of which decreases the electric field at these locations. In addition, x-ray images of the electron beam demonstrate that the cross-sectional uniformity of the electron beam (see Fig. 14(b)) is improved in comparison with the cathode without screening electrode. X-ray patterns of the electron beam generated in the presence of a guiding magnetic field $B = 3$ kG, showed a slightly smaller diameter, $\sim$2.6 cm, than that of the

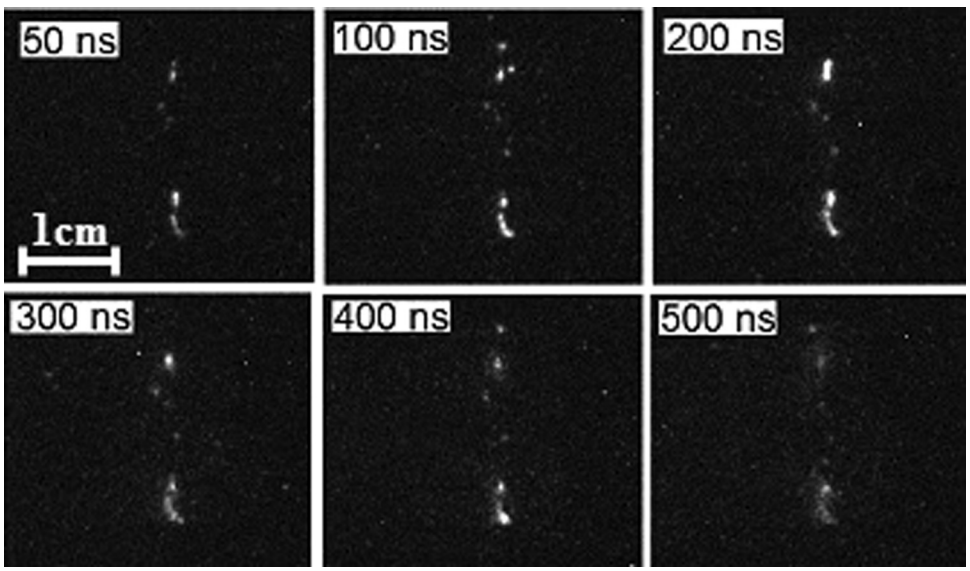

FIG. 11. Framing (20 ns in duration) images of the light emission from the cathode plasma in the case of the coaxial diode obtained at different time delays with respect to the beginning of the accelerating pulse. $B \approx 3$ kG.

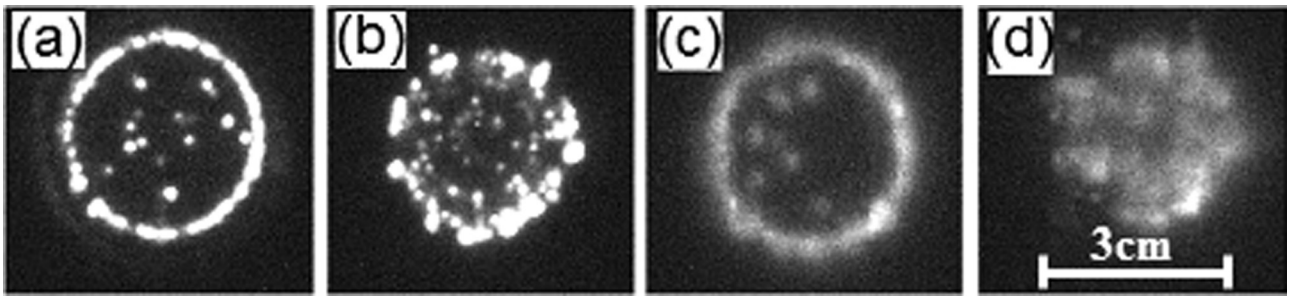

FIG. 12. Typical front images of light emission from the carbon (a) and aluminum (b) cathodes; typical x-ray images of the electron beam: (c) carbon cathode, (d) aluminum cathode. $\tau_d \approx 150$ ns. A Mo foil collector was behind the anode grid, $B \approx 3$ kG, $d_{Ak} = 1$ cm, frame duration 20 ns, $\varphi_{AK} \approx 150$ kV.

cathode. This can also be explained by the decreased electric field at the peripheral carbon fiber-epoxy, due to the screening electrode. Here it should be noted that, in spite of the improved cross-sectional uniformity of the electron beam current density, this cathode has a limited lifetime because EE centers form after ~20 generator shots on the surface of the screening electrode, which was located at a distance of ~7 mm from the anode grid (average electric field of 220 kV/cm). Additional measures should be taken to avoid this phenomenon.

C. Spectroscopic studies of the cathode and anode plasmas

The cathode and anode plasma parameters at different distances from the cathode were determined using non-disturbing time- and space-resolved spectroscopy (see Sec. II). In the experiments described in this section, the experimental conditions were $d_{AK} \approx 10$ mm, $\varphi_{AK} \approx 150$ kV, diode current of ~ 3 kA, and $B \approx 3$ kG.

1. Temporal evolution of spectral lines

First let us note the good reproducibility of the different spectral line intensities obtained at the output of the spectrometer by the PMT. Nevertheless, waveforms of the spectral line intensity were averaged over five different shots and the resulting curve was smoothed in order to avoid noise oscillations in the range above1 GHz. Here let us note that a rough estimate showed that this optical setup allows us to observe plasma with a density $\geq 5 \times 10^{12}$ cm^{-3}. The plasma was found to be composed of hydrogen atoms along with protons and singly and doubly ionized carbon ions, which indicates a rather large temperature of plasma electrons (*C* III requires plasma electrons with energy ≥24.5 eV).

Typical temporal behavior of *C* II ion spectral line intensity at different distances from the cathode is shown in Fig. 15. The almost identical intensities at 0 mm and 2 mm from the cathode can be explained by the curvature of the cathode. One can see a drastic decrease in the *C* II spectral line intensity at a distance of 4 mm, which indicates a steep decrease in the plasma density. In addition, a time delay of $\sim 170 \pm 30$ ns in the appearance of this line is observed, which corresponds to a cathode plasma velocity $v_{pl} = (1.5 \pm 0.3) \times 10^6$cm/s. Qualitatively, the same temporal evolution was obtained for the H_β spectral line intensity, which also results in a hydrogen atom propagation velocity $v_H \approx (1.6 \pm 0.3) \times 10^6$ cm/s. The appearance of the H_β spectral line at different distances from the cathode was also measured using a 4Quik05A framing camera. These measurements agreed well with the above results obtained using the PMT. Thus, one can conclude that the expansion of the plasma occurs with the same velocity for the hydrogen and the carbon ions. Let us note that the spectral line of *C* III ($\lambda = 4068.91$ Å) was obtained only in the vicinity of the carbon-epoxy capillaries, which also indicates a drastic

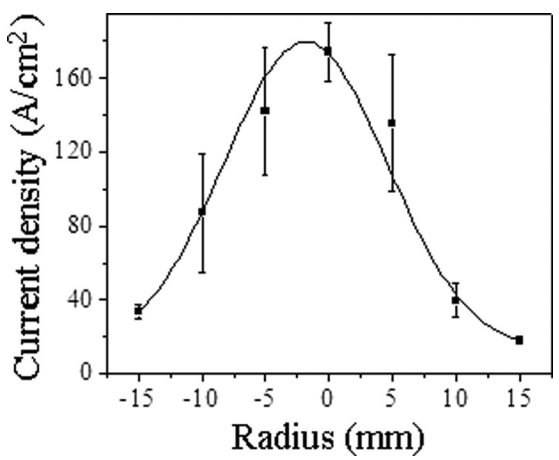

FIG. 13. Radial distribution of the electron beam current density for carbon-epoxy capillary cathode. $\tau_d \approx 80$ ns with respect to the beginning of the accelerating pulse, $B \approx 3$ kG, $d_{AK} = 10$ mm, $\varphi_{AK} \approx 150$ kV. CFCs were placed behind the anode grid at a distance of 5 mm. The cathode design is shown in Fig. 1(a).

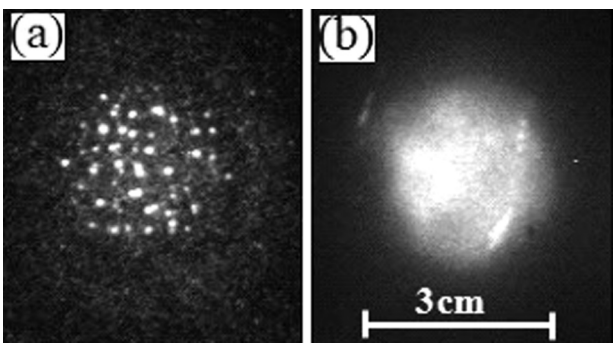

FIG. 14. (a) Typical front image of light emission from the carbon-epoxy capillary cathode, (b) typical x-ray image of the electron beam. (a) $\tau_d \approx 48$ ns, (b) $\tau_d \approx 60$ ns. A Mo foil collector with scintillator was behind the anode grid, $B \approx 3$ kG, $d_{ac} \approx 1$ cm. The frame duration is of 20 ns, $\varphi_{ac} \approx 150$ kV. The cathode is shown in Fig. 1(b).

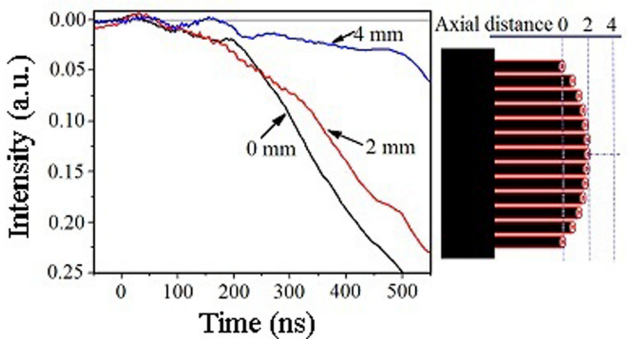

FIG. 15. Intensity of *C* II spectral line $\lambda = 4267.26$ Å versus time for three different axial positions.

decrease in the cathode plasma density versus the distance from the cathode.

The anode plasma formation was also studied with the spectrometer and PMT at its exit. The obtained H_β, *C* II, and *C* III spectral line intensities revealed that the anode plasma appears at $\tau_d \sim 200$ ns at a distance of 1 mm from the anode grid. Calculations of the electron beam energy deposition into the anode grid show that the threshold for plasma formation of ~0.1 kJ/g,[7,47] is reached at $\tau_d \sim 100$ ns. Thus, one can estimate the anode plasma velocity to be $\sim 10^6$ cm/s. The existence of hydrogen and carbon ions in the anode plasma is explained by the ionization of the desorbed surface monolayers from the surface of the anode grid. Here, let us note that the intensity of the H_β spectral line was significantly smaller than in the case of the cathode plasma and not enough to estimate the plasma density using Stark broadening analysis. In addition, a drastic increase in the intensity of different spectral lines was obtained at $\tau_d \approx 500$ ns. This phenomenon was also obtained at all the other distances studied inside the AK gap. This drastic simultaneous increase in spectral line intensity coincides with the time at which the accelerating pulse is terminated and can be explained by overlapping between the propagating dilute cathode and anode plasmas at that time. The drastic increase in the spectral line intensities cannot be explained by a quick increase in the plasma density throughout the entire AK gap. It can, however, be explained by a fast increase in the plasma electron temperature and, a corresponding increase in the excitation cross-section at the time when the AK gap is shortened due to Joule heating of the plasma electrons by the current that continues to flow through the plasma. Indeed, it was obtained that the peaks in the intensity of the spectral lines coincide with the peaks of the ringing diode current (by the time the diode short-circuited, 30% of the stored energy remained in the HV generator). This explanation also agrees with the sharp increase in the spectral line of the CIII ($\lambda = 4068.91$ Å) ions, the intensity of which was negligible prior to the AK gap shorting at that position, that was obtained in the middle of the AK gap (~5 mm away from the both anode and cathode).

Finally, in Fig. 16, one can see a steep decrease in the intensity of the different spectral lines in relation to the distance from the cathode, which becomes practically invisible at ~2mm from the cathode. This also indicates a fast decrease in the cathode plasma density, assuming that the plasma electron temperature within the gap remains approximately constant. Thus, one can suppose that the bulk of the cathode dense plasma remains in the vicinity of the cathode and that only dilute plasma propagates toward the anode.

2. Spectral line broadening measurements

The plasma electron density n_e, electron temperature, and hydrogen temperature, were studied using the Stark and Doppler broadening analysis of the H_α and H_β spectral lines and collision-radiative modeling (CRM).[44] Measurements of the spectral line broadening were taken at different axial positions from the cathode, 1 mm apart, until the signal became unresolvable. In these experiments, the entrance slit of the spectrometer was 50μm and the exposure time of the fast framing camera was 100 ns. The spectral line profiles were averaged over at least 10 shots and the error bars in FWHM and intensity was ±2% and ±5%, respectively. The H_α spectral line width was measured at different axial positions and at two different time intervals during the accelerating pulse. The hydrogen atom temperature was calculated from Doppler broadening assuming an insignificant Stark effect for this transition. This assumption can be considered as reasonable for the H_α spectral line when a high frequency ($>10^{11}$ s^{-1}) electric field is absent and the plasma density is $\leq 5 \times 10^{15}$ cm^{-3}.[48] These measurements show that the hydrogen atoms' temperature is approximately constant at different distances from the cathode and reaches a rather large value of 4.7 ± 0.2 eV at $\tau_d = 250 \pm 50$ ns; it decreases to 3.7 ± 0.2 eV at $\tau_d = 350 \pm 50$ ns. In general, the obtained hydrogen atoms' temperature could not be used to determine the plasma ion temperature in the case of a plasma density $\leq 10^{15}$cm^{-3} because of the low ion-neutral collisional frequency, which is $\sim 10^7$ s^{-1} for a particles' velocity of $\sim 10^6$ cm/s, and a collision cross-section of $\sim 10^{-15}$cm^2. However, in our case one can consider that the plasma ions obtain the same temperature as that of the hydrogen atoms. Indeed, rough estimates show that the density of the plasma

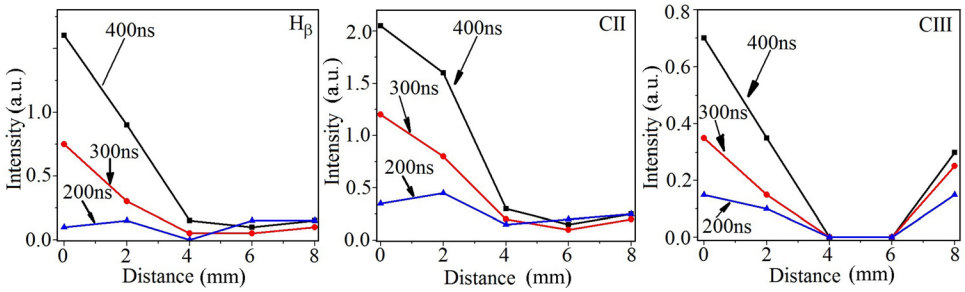

FIG. 16. Temporal evolution of H_β, *C* II ($\lambda = 4267.26$ Å) and CIII ($\lambda = 4068.91$ Å) spectral lines intensity versus the distance from the cathode.

generated inside the capillary should be $\geq 3 \times 10^{16}\,\mathrm{cm}^{-3}$, which results in an ns time scale of ion-neutral collision frequency, and a corresponding fast ion-neutral thermalization. Nevertheless, the analysis of the spectral line broadening of C II ions was carried out. This analysis revealed that the spectral lines of CII ions have a FWHM of ~1 Å, which corresponds to an unreasonable ion temperature of >300 eV. Moreover, at a distance of 1 mm from the edge of the central part of the cathode, the spectral lines exhibited two resolvable peaks (see Fig. 17). This structure of the spectral lines ($\lambda = 3918.98$ Å and $\lambda = 3920.69$ Å) cannot be related to either Zeeman or Stark splitting, since their effects are negligibly small for the present experimental conditions, in comparison with the observed splitting. In addition, ion cyclotron rotation can be excluded as a reason for the peaks that were observed because this effect would lead to line broadening; also, it should be observed at all distances from the cathode. Let us also note that these two peaks could not be explained by the plasma opacity either, because, as will be shown, the plasma density and typical dimension do not exceed $2 \times 10^{15}\,\mathrm{cm}^{-3}$and 3 cm, respectively. One can suppose that a fast radial expansion of dense plasma flow ejected from the capillary is responsible for the obtained splitting of the CII spectral lines at that distance. Since the distance between capillaries is 1.5 mm, the overlapping between neighboring plasma flows occurs at a small distance from the capillaries' tips, leading to ion thermalization by collisions and, correspondingly, to a decrease in the radial expansion velocity. The same concerns can be applied for the broadening of the H_α spectral line, which was assumed to be purely thermal. Thus, the obtained temperature of 4.7 eV can be considered only as an upper limit of the neutrals and ions' temperature.

The H_β spectral line intensity was measured at the same locations and times as the H_α spectral line. Using the Doppler broadening of the H_α spectral line, the FWHM of the Stark broadening of the H_β spectral line was determined and used to calculate the plasma electron density. In these calculations, the effects of electron impact and ion dynamics were neglected, which can be considered as reasonable

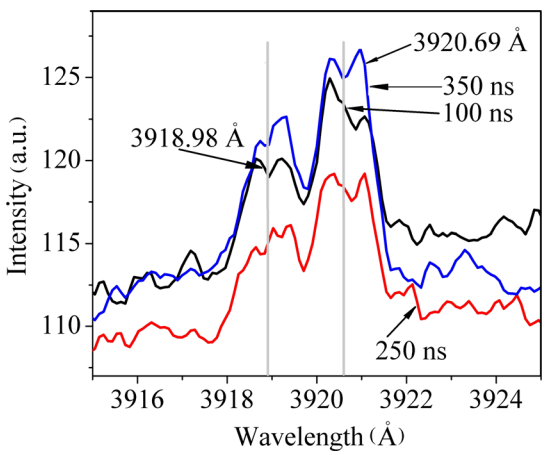

FIG. 17. Splitting in the intensity profile of the *C* II spectral lines at 1 mm from the cathode surface at different time delays with respect to the beginning of the accelerating pulse.

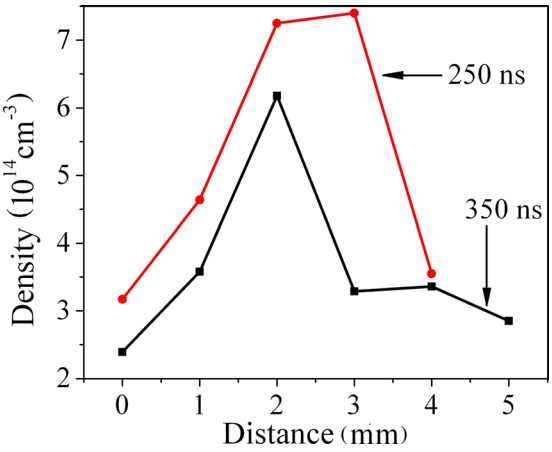

FIG. 18. Plasma electron density versus the distance from the cathode for two different time intervals during the accelerating pulse.

assumptions for plasma of densities of $<10^{16}\,\mathrm{cm}^{-3}$.[48] The electron density distributions versus the distance from the cathode at two different time intervals during the accelerating pulse are shown in Fig. 18. One can see that the densest (up to $8 \times 10^{14}\,\mathrm{cm}^{-3}$) plasma forms in the vicinity of the cathode, at ~1 mm from the edge of the central part of the cathode, with a following steep decrease. This maximum in the plasma density at that distance can be explained by the overlapping of conical plasma flows generated by separate capillaries.[49] At $\tau_d > 300$ ns, plasma with a density of $\sim 3 \times 10^{14}\,\mathrm{cm}^{-3}$ was obtained also at distances up to 3 mm (in Fig. 18 this distance corresponds to 5 mm) from the edge of the central part of the cathode. However, at distances larger than 4 mm (in Fig. 18 this corresponds to distances larger than 6 mm) the intensity of the H_β spectral line becomes negligibly small, which indicates that the plasma density at those locations does not exceed $\sim 10^{13}\,\mathrm{cm}^{-3}$.

The plasma electron temperature, T_e was determined using a comparison between the measured and simulated (by CR modeling) H_β/H_α ratio. The input parameters for the time-dependent CR modeling were the plasma density and electron temperature. It was shown that within the studied ranges of the plasma parameters (density range $10^{14} - 10^{16}\,\mathrm{cm}^{-3}$and temperature range 4 – 13 eV), a steady state Boltzmann distribution of excited energy levels population does not exist and one has to take into account the time dependence of the energy state population. For instance, even for $n_e = 10^{16}\,\mathrm{cm}^{-3}$ and $T_e = 13$ eV, a steady state of the energy level population was obtained only at $\tau_d > 100$ ns. The best fit between the simulated and experimental H_β/H_α ratio was found for plasma electron temperature in the range 11 – 13 eV for plasma density in the range (5–10) $\times 10^{14}\,\mathrm{cm}^{-3}$ (see, example in Fig. 19). This rather large electron temperature agrees with the presence of the *C* III ions that were already observed in the cathode plasma at $\tau_d \sim 100$ ns.

D. Electron beam transport in guiding magnetic field

The dependence of the amplitude of the electron beam current on the value of the external magnetic field obtained at a distance of 5 mm from the anode grid using a CFC placed behind the anode grid is shown in Fig. 20. One can

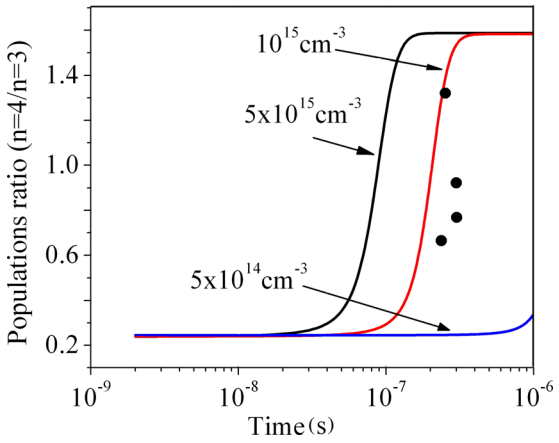

FIG. 19. Comparison between the CR simulated and experimental H_α/H_β ratio for $n_e = 10^{15}$ cm^{-3} and $T_e = 11$ eV. Lines – simulation; Dots – experiment.

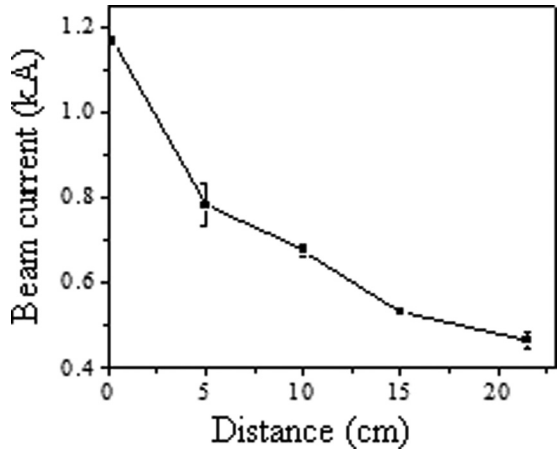

FIG. 21. Dependence of the electron beam current amplitude versus the distance from the anode grid. $d_{AK} \approx 1.4$ cm, $\varphi_{AK} \approx 180$ kV, $B = 3$ kG.

see that an increase in the magnetic field from 0.3 kG to 2.5 kG leads to an increase in the electron beam current amplitude registered by the CFC from 0.68 kA to ~1.2 kA. This can be explained by the decrease in the beam divergence that is typical for carbon fiber emitters[23] due to electron magnetization, leading to the formation of a rigid electron beam. The increase in the magnetic field from 2.5 kG up to 4 kG does not change the beam amplitude, and a further increase in the value of B even shows a decrease in the value of I_d. The latter can be explained by the decrease in the plasma transverse expansion and, correspondingly, the decrease in the effective plasma emission cross-sectional area.

In general, an electron beam that is generated in the presence of a guiding magnetic field and injected without its space charge neutralization into a vacuum drift space is characterized by its azimuthal rotation during its axial propagation. The dependence of the electron beam current amplitude versus the propagation distance L with respect to the anode grid in the guiding uniform magnetic field $B = 3$ kG shows a fast decrease in the electron beam current from ~1160 A behind the anode grid down to ~470 A at a distance of 21.5 cm from it (see Fig. 21). This decrease in the beam current cannot be explained by the beam self-space charge Coulomb repulsion because the energy density of the magnetic field significantly exceeds (~10 times) the energy density of beam particles:[45] $B^2/8\pi > n_e m_e c^2 \gamma$, where $n_e \approx 5 \cdot 10^{10}$ cm^{-3} is the electron beam density, and c is the light velocity. Thus, the decrease in the beam current amplitude is related to the formation of the virtual cathode (VC). Indeed, injection of an electron beam with non-compensated space charge and radius r_b into a vacuum drift tube with radius r_t and having a current amplitude larger than the critical current amplitude[44] $I_{cr} = 17(\gamma^{2/3} - 1)^{3/2}/[1 + 2\ln(r_t/r_b)] \approx 0.58$ kA leads to the formation of a VC at a typical distance from the anode grid which is comparable with the value of d_{AK} and with the depth of the potential well, $\varphi_{VC} \simeq 510(\gamma - \gamma^{1/3}) \approx 130$ kV.[46] Finally, the cross-sectional distribution of the electron beam current density at different distances L from the anode grid was studied using x-ray images captured by a 4Quik05A camera. It was found that the electron beam changes its structure from solid at the entrance to the drift tube to hollow during its propagation. Namely, at a distance $L \geq 5$ cm one already obtains a hollow structure of the electron beam current density radial distribution (see Fig. 22).

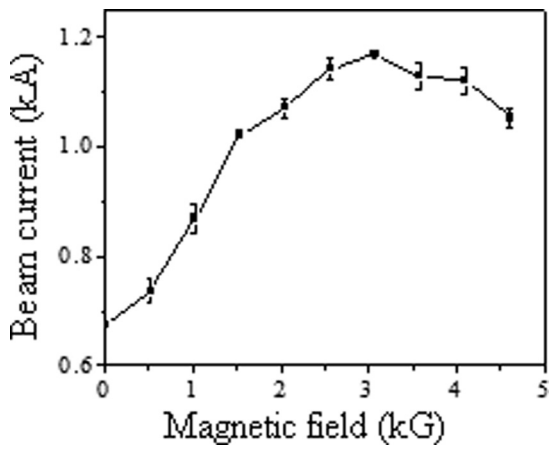

FIG. 20. Dependence of electron beam current on magnetic field. $d_{ac} = 1.4$ cm, $\varphi_{AK} \approx 175$ kV.

IV. DISCUSSION

In this section, let us discuss the hollow structure of the electron beam during its transport in the guiding magnetic field in the drift tube. Let us consider a solid electron beam of radius r_b injected into a metallic chamber of radius r_t, through a grounded anode grid. It is assumed that a guiding magnetic field is rather strong and prevents the radial motion of the beam electrons. A radial potential well, $\varphi(r,z)$, which is formed by the beam space charge, affects the longitudinal motion of the electrons. Far from the anode grid, the potential $\varphi(r,z)$ does not depend on the longitudinal coordinate z. When the beam current is so large that at a certain radius, r_c, the potential barrier, $|\varphi(r_c)|$, exceeds the beam accelerating voltage, φ_{AK}, the electrons whose injection radius, r_0, is smaller than r_c cannot overcome the barrier and turn back to the injection plane, whereas peripheral electrons continue

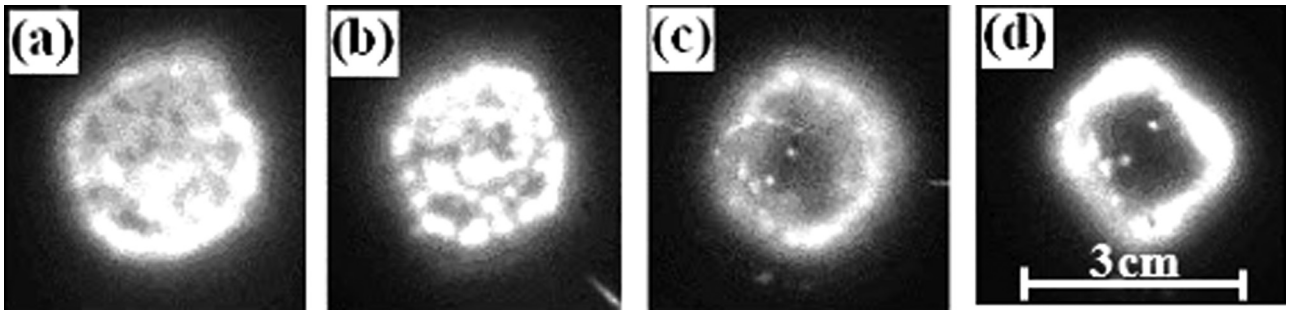

FIG. 22. X-ray images of electron beams at different distances from the anode grid. Frame duration is of 20 ns. (a) behind the anode grid, (b) $L = 2$ cm, (c) $L = 5$ cm, and (d) $L = 15$ cm. Time delay with respect to the beginning of the accelerating pulse is $\tau_d \approx 80$ ns, $B \approx 3$ kG, $d_{ac} \approx 1$ cm, $\varphi_{AK} \approx 150$ kV.

their motion along the chamber. In such a way, a hollow beam can be formed when the injection current I_b exceeds some critical value I_{cr} the value of which can be estimated as follows.

The continuity equation, $n(r,z)v(r,z) = n(r,0)v(r,0) = n_0(r)v_0(r)$ and the energy conservation law, $mv^2(r,z)/2 - e\varphi(r,z) = e\varphi_{AK}$ allow the Poisson equation to be presented as,

$$\frac{1}{r}\frac{d}{dr}\left(r\frac{d\varphi}{dr}\right) = \frac{4\pi e n_0(r)}{\sqrt{1+\varphi(r)/\varphi_{AK}}}, \quad (1)$$

Here $n_0(r)$ and $v_0(r)$ are the radial distribution of the beam density and velocity at the injection plane. Eq. (1) is valid far from the grid, where the potential is independent on z. This equation can be written in the dimensionless form

$$\frac{1}{\rho}\frac{d}{d\rho}\left(\rho\frac{d\psi}{d\rho}\right) = \frac{I_A I(\rho)}{\psi_b^{3/2}}\frac{1}{1+\psi(\rho)}, \quad (2)$$

where $\rho = r/r_b$, $\psi = \varphi/\varphi_{AK}$, $I(\rho) = I_b$ if $\rho < 1$, and $I(\rho) = 0$ if $\rho > 1$, $I_A = m_e c^3/e$, and $\psi_b = e\varphi_{AK}/2mc^2$. If Eq. (2) has a solution that satisfies the boundary conditions $\psi(\rho_t) = 0$ (here $\rho_t = r_t/r_b$) and $(d\psi/d\rho)_{\rho=0} = 0$, the beam propagates as a whole through the chamber. Otherwise, only the peripheral part of the beam can be transported through the chamber, whereas the central part of the beam is reflected back. The numerical solution of Eq. (2) with experimental values of the parameters ($\varphi_{ac} \approx 150$ kV, $r_t/r_b = 3$) shows that the central part of the beam is reflected back when the beam current exceeds 0.5 kA, which agrees rather well with the experimental data.

V. SUMMARY

It was found that the carbon fiber-epoxy cathode can be used for reliable generation of electron beams with $j_e \approx 300$ A/cm^2 at accelerating voltages of ≤ 200 kV [average value and rise time of the diode electric field are ≤ 200 kV/cm and $\leq 10^{13}$ V/(cm·s), respectively], pulse duration up to ~450 ns with a satisfactorily uniform cross-sectional distribution of the electron beam current density. It was shown that the electric field threshold for the beginning of the electron emission is ≤ 15 kV/cm and that this cathode can sustain ~3000 generator pulses without any degradation in its emission properties.

The phenomenon governing the electron emission is flashover plasma, which is formed along the internal surface of the carbon-epoxy capillaries tube during the fast rise time of the accelerating voltage. These plasma flows generated by separate capillaries overlap one another at a distance of ~1 mm from the cathode capillaries. The time- and space-resolved visible light observation and spectroscopy analysis showed that the cathode plasma in the vicinity of the cathode capillaries is characterized by $n_e \leq 10^{15}$ cm^{-3}, $T_e \leq 13$ eV, $T_i \leq 4$ eV. It was shown that the cathode plasma density decreases steeply with the distance from the cathode, and the average axial expansion velocity of the plasma does not exceed 1.6×10^6 cm/s. In addition, it was found that the main reason for the short-circuit of the AK gap is the early formation of the anode plasma and its expansion towards the cathode plasma.

Finally, it was shown that the injection into the drift space of the electron beam with a current amplitude exceeding its critical value leads to the VC formation and changes the cross-sectional radial distribution of the electron beam current density because inner electrons are reflected from the VC.

ACKNOWLEDGMENTS

This research was supported by the Center for Absorption in Science, Ministry of Immigrant Absorption, State of Israel.

[1]R. B. Miller, *Introduction to the Physics of Intense Charged Particle Beams* (Plenum, New York, 1982).
[2]V. I. Engelko, Plasma Devices Oper. **13**, 135 (2005).
[3]R. H. Fowler and L. Nordheim, Proc. R. Soc. London, Ser. A **121**, 626 (1928).
[4]G. A. Mesyats, *Explosive Electron Emission* (URO, Ekaterinburg, 1998).
[5]S. Dushman, Phys. Rev. **21**, 623 (1923).
[6]A. S. Gilmour, Jr., *Microwave Tubes* (Artech House, Norwood, MA, 1986).
[7]F. J. Agee, IEEE Trans. Plasma Sci. **26**, 235 (1998).
[8]J. W. Luginsland, Y. Y. Lau, and R. M. Gilgenbuch, Phys. Rev. Lett. **77**, 4668 (1996).
[9]J. J. Watrous, J. W. Luginsland, and M. H. Freese, Phys. Plasmas **8**, 4202 (2001).
[10]S. Ya. Belomytsev, S. D. Korovin, and I. Pegel, IEEE Trans. Plasma Sci. **27**, 1572 (1999).
[11]Ya. E. Krasik, J. Z. Gleizer, D. Yarmolich, V. Vekselman, Y. Hadas, A. Krokhmal, K. Chirko, O. Peleg, and J. Felsteiner, IEEJ Trans. Fundam. Mater. **127**, 697 (2007).
[12]Ya. E. Krasik, D. Yarmolich, J. Z. Gleizer, V. Vekselman, Y. Hadas, V. Tz. Gurovich, and J. Felsteiner, Phys. Plasma **16**, 057103 (2009).
[13]E. Oks, *Plasma Cathode Electron Sources* (Willey-VCH, Weinheim, 2006).
[14]G. Rosenman, D. Shur, Ya. E. Krasik, and A. Dunaevsky, J. Appl. Phys. **88**, 6109 (2000).

[15]Ya. E. Krasik, K. Chirko, A. Dunaevsky, J. Felsteiner, A. Krokhmal, J. Gleizer, A. Sayapin, and J. Felsteiner, IEEE Trans. Plasma Sci. **31**, 49 (2003).
[16]J. Z. Gleizer, D. Yarmolich, V. Vekselman, J. Felsteiner, and Ya. E. Krasik, Plasma Devices Oper. **14**, 223 (2006).
[17]V. Vekselman, J. Z. Gleizer, S. Yatom, V. Tz. Gurovich, and Ya. E. Krasik, J. Appl. Phys. **108**, 093303 (2010).
[18]A. Dunaevsky, Ya. E. Krasik, and J. Felsteiner, and A. Sternlieb, J. Appl. Phys. **90**, 3689 (2001).
[19]J. Z. Gleizer, K. Chirko, D. Yarmolich, S. Efimov, and Ya. E. Krasik, Eur. Phys. J.: Appl. Phys. **34**, 35 (2006).
[20]J. Z. Gleizer, A. Krokhmal, Ya. E. Krasik, and J. Felsteiner, Eur. Phys. J. D **26**, 285 (2003).
[21]A. Krokhmal, J. Z. Gleizer, Ya. E. Krasik, V. Ts. Gurovich, and J. Felsteiner, J. Appl. Phys. **95**, 3304 (2004).
[22]A. Krokhmal, J. Z. Gleizer, Ya. E. Krasik, V. Ts. Gurovich, and J. Felsteiner, Europhys. Lett. **66**, 226 (2004).
[23]G. A. Mesyats and D. I. Proskurovsky, *Pulsed Electrical Discharges in Vacuum* (Springer, Berlin, 1989).
[24]Ya. E. Krasik, A. Dunaevsky, A. Krokhmal, J. Felsteiner, A. V. Gunin, I. V. Pegel, and S. D. Korovin, J. Appl. Phys. **89**, 2379 (2001).
[25]S. P. Bugaev, G. A. Mesyats, and D. I. Proskurovsky, Sov. Phys. Dokl. **14**, 605 (1969).
[26]G. A. Mesyats and D. I. Proskurovsky, JETP Lett. **13**, 4 (1971).
[27]Ya. E. Krasik, A. Dunaevsky, and J. Felsteiner, Eur. Phys. J. **D15**, 345 (2001).
[28]R. Prohaska and A. Fisher, Rev. Sci. Instrum. **51**, 1092 (1980).
[29]J. G. Eden and D. Epp, Rev. Sci. Instrum. **53**, 781 (1980).
[30]V. A. Burtsev, M. A. Vasilevskii, Yu. A. Vasilevskaya, I. M. Roife, V. I. Engel'ko, S. P. Yakovlev, and E. G. Yankin, Sov. Phys. Tech. Phys. **26**, 847 (1981).
[31]E. Garate, R. D. McWilliams, D. E. Voss, A. L. Lovesee, K. J. Hendricks, T. A. Spencer, M. C. Clark, and A. Fisher, Rev. Sci. Instrum. **66**, 2528 (1995).
[32]R. B. Miller, J. Appl. Phys. **84**, 3880 (1998).
[33]D. A. Shiffler, M. J. LaCour, M. D. Sena, M. D. Mitchell, M. D. Haworth, K. J. Hendricks, and T. A. Spencer, IEEE Trans. Plasma Sci. **28**, 517 (2000).
[34]D. Shiffler, M. LaCour, K. Golby, M. Sena, M. Mitchell, M. Haworth, K. Hendricks, and T. Spencer, IEEE Trans. Plasma Sci. **29**, 445 (2001).
[35]Yu. M. Saveliev, W. Sibbet, and D. Parkes, Appl. Phys. Lett. **81**, 2343 (2002).
[36]Ya. E. Krasik, A. Dunaevsky, J. Felsteiner, J. Z. Gleizer, Yu. A. Kotov, S. Yu. Sokovnin, and M. E. Balezin, J. Appl. Phys. **91**, 9385 (2002).
[37]D. Shiffler, M. Ruebush, D. Zagar, M. LaCour, M. Sena, K. Golby, M. Haworth, and R. Umstattd, J. Appl. Phys. **91**, 5599 (2002).
[38]Yu. M. Saveliev, W. Sibbett, and D. M. Parkes, J. Appl. Phys. **94**, 7416 (2003).
[39]D. Shiffler, J. Heggemeier, M. LaCour, K. Golby, and M. Ruebush, Phys. Plasmas **11**, 1680 (2004).
[40]M. Friedman, M. Myers, F. Hegeler, S. B. Swanekamp, M. F. Wolford, J. D. Sethian, and L. Ludekingd, J. Appl. Phys. **96**, 7714 (2004).
[41]J. Z. Gleizer, Y. Hadas, D. Yarmolich, J. Felsteiner, and Ya. E. Krasik, Appl. Phys. Lett. **90**, 181501 (2007).
[42]Ya. E. Krasik, J. Z. Gleizer, D. Yarmolich, A. Krokhmal, V. Ts. Gurovich, E. Efimov, J. Felsteiner, V. Bernshtam, and Yu. M. Saveliev, J. Appl. Phys. **98**, 093308 (2005).
[43]V. Vekselman, J. Gleizer, D. Yarmolich, J. Felsteiner Ya. Krasik, L. Liu, and V. Bernshtam, Appl. Phys. Lett. **93**, 081503 (2008).
[44]Yu. V. Ralchenko and Y. Maron, J. Quant. Spectrosc. Radiat. Transf. **71**, 609 (2001).
[45]L. S. Bogdankevich and A. A. Ruchadze, Sov. Phys. Usp. **14**, 163 (1971).
[46]E. A. Abramyan, B. A. Alterkop, and G. D. Kuleshov, *Intense Electron Beams* (Energoatomizdat, Moscow, 1984).
[47]J. Benford and G. Benford, IEEE Trans. Plasma Sci. **25**, 311 (1997).
[48]H. R. Griem, *Spectral Line Broadening by Plasma* (Academic, New York, 1974).
[49]J. Z. Gleizer, Y. Hadas, D. Yarmolich, J. Felsteiner, and Ya. E. Krasik, J. Appl. Phys. **103**, 043302 (2008).